International Journal of Pharmaceutics 575 (2020) 118961

Contents lists available at ScienceDirect

International Journal of Pharmaceutics

journal homepage: www.elsevier.com/locate/ijpharm

Targeted ErbB3 cancer therapy: A synergistic approach to effectively combat cancer

Muhammad Yasir Ali[a,b], Imran Tariq[a,c], Sajid Ali[a], Muhammad Umair Amin[a], Konrad Engelhardt[a], Shashank Reddy Pinnapireddy[a], Lili Duse[a], Jens Schäfer[a], Udo Bakowsky[a,*]

[a] Department of Pharmaceutics and Biopharmaceutics, University of Marburg, Marburg, Germany
[b] Faculty of Pharmaceutical Sciences, GC University Faisalabad, Faisalabad, Pakistan
[c] Punjab University College of Pharmacy, University of the Punjab, Lahore, Pakistan

ARTICLE INFO

Keywords:
Sorafenib
Aptamer
Nanoparticles
Cytotoxicity
PLGA

ABSTRACT

Surface modification of nanoparticles with aptamer is gaining popularity lately due to its selective targeting and low immunogenicity. In this study, sorafenib tosylate (SFB) was loaded in biodegradable PLGA nanoparticles prepared by solvent evaporation method. The surfaces of drug deprived and drug-loaded particles (PN and PNS, respectively) were coupled with aptamer to target ErbB3 using EDC/NHS chemical modification. Nanoparticles were characterized with regard to their size, shape and chemical composition by dynamic light scattering, atomic force microscopy, FTIR and elemental analysis respectively. To evaluate the particles in vitro cell culture studies were performed. Cell viability assay, pathway analysis and apoptosis assay showed cellular toxicity in the presence of aptamer in PNS-Apt ($p < 0.001$). Metastatic progression assay showed decreased cell migration in the presence of aptamer and SFB. Confocal laser scanning microscopy was used to visualize the receptor-mediated time-dependent intracellular uptake and distribution of the nanoparticles throughout the cytoplasm. The findings of the current study demonstrated the potential efficacy of the surface modified SFB-loaded particles against ErbB3.

1. Introduction

Non-specificity of the chemotherapeutic agents has triggered the use of targeted drug delivery approaches to reduce normal tissue toxicity (Farokhzad et al., 2006; Aravind et al., 2012). The development of nanoparticles and liposomes has changed the face of chemotherapy. Therapeutic agents can be loaded in nanoparticles by entrapment or encapsulation (Muthu and Singh, 2009; Dinarvand et al., 2011). Poly-lactide-co-glycolide (PLGA), polylactic acid (PLA) and polyglycolic acid (PGA) are the most commonly used materials for the preparation of nanoparticles, due to their biocompatibility and biodegradability. Among these, PLGA is one of the most commonly used materials for the preparation of nanoparticles. Development of nanoparticles with a functionalized tumor-specific ligand that can selectively target the tumor tissues remains one of the main challenges (Farokhzad et al., 2006; Dinarvand et al., 2011).

Aptamers are short sequence RNA or DNA, which can bind, like an antibody, with high specificity to the target molecules, cells or tissues. However, aptamers are superior as compared to the antibodies due to their chemical synthesis, ease of modification, little batch-to-batch variation and physical stability (Plourde et al., 2017; Wu et al., 2015; Ozalp et al., 2011). Different approaches regarding the use of aptamers have been developed for the treatment of different diseases, including their use as a single therapeutic agent against the target moiety or as a drug conjugate. One major drawback with the use of aptamers is their degradation by nucleases. This can be addressed by immobilizing them on the surface of nanoparticles (McKeague and DeRosa, 2012; Jo and Ban, 2016).

Many tumor cells are rich in receptor tyrosine kinases (RTK), responsible for different cell cycles by their intracellular kinase domain. There is a well-known mechanism of receptor-mediated endocytosis of ligands binding to RTK, by clathrin-dependent mechanism. These receptors are internalized in the presence of an aptamer to form endosomes and are subsequently degraded inside lysosomes (Graphical Abstract). These aptamers then inhibit cytoplasmic cascade of reactions (Szymanska et al., 2016; Belleudi et al., 2012; Roepstorff et al., 2008). The hydrolysis in lysosome results in the subsequent release of the therapeutic agent inside the cytoplasm.

The aim of the current study was to design an anti-ErbB3-aptamer (Chen et al., 2003) modified sorafenib tosylate loaded nanoparticles.

* Corresponding author at: Department of Pharmaceutics and Biopharmaceutics, University of Marburg, Robert-Koch-Str. 4, 35037 Marburg, Germany.
E-mail addresses: bakowsky@staff.uni-marburg.de, ubakowsky@aol.com (U. Bakowsky).

https://doi.org/10.1016/j.ijpharm.2019.118961
Received 9 August 2019; Received in revised form 9 December 2019; Accepted 12 December 2019
Available online 14 December 2019
0378-5173/

SFB is a multi-kinase inhibitor, which blocks VEGFR (another RTK). This inhibition results in the blockage of angiogenesis and cell proliferation (Guo et al., 2017; Broecker-Preuss et al., 2015). One of the drawbacks of SFB therapy is resistance due to non-specific drug delivery. Therefore, the nanoparticles were surface modified with aptamer to overcome this problem (Zhai et al., 2014). The prepared nanoparticles were then characterized by dynamic light scattering, atomic force microscopy, FTIR and elemental analysis. These formulations were further characterized in vitro for cell viability, pathway analysis and cellular uptake. The oxidative stress in the presence of these nanoscaled formulations was also evaluated.

2. Materials and methods

2.1. Materials

RNA aptamer, (Apt) with 5′ cyanine 5 (Cyn 5) and 3′ C6 amino modifier spacer group (5′-CAGCGAAAGUUGCGUAUGGGUCACAUCG CAG-3′) was purchased from Eurogentec (Seraing, Belgium). PLGA (R503H, 30 kDa) was obtained from Evonic (Darmstadt, Germany). 1-ethyl-3-(3-dimethylaminopropyl)- carbodiimide (EDC), N-hydroxysuccinimide (NHS), 3-(4,5-dimethyl-2-thiazolyl)-2,5-diphenyl-2H-tetrazolium bromide (MTT), 2′,7′-dichlorofluorescein diacetate (DCFDA) and *tert*-butyl hydroperoxide (TBHP) were purchased from Sigma Aldrich (Darmstadt, Germany). 2-(*N*-morpholino) ethanesulfonic acid (MES) was purchased from Serva (Heidelberg, Germany). Polyvinyl-alcohol (Mowiol 4-88) was a gift sample from Kuraray (Hattersheim, Germany). Sorafenib tosylate was purchased from LC Laboratories (Woburn, USA). Ethyl acetate, tetrahydrofuran and ethanol were obtained from Chemsolute-Th. Geyer (Renningen, Germany), Carl Roth (Karlsruhe, Germany) and Fischer Scientific (Schwerte, Germany) respectively. All the reagents used were of analytical grade.

2.2. Cell lines and cell culture

ErbB3 positive human breast cancer cell line MDA-MB-231 was purchased from ATCC Manassas, USA. Cells were grown in RPMI:DMEM (50:50) (Capricorn Scientific, Ebsdorfergrund, Germany) supplemented with 10% fetal bovine serum (Sigma Aldrich). Cells were cultivated in humid conditions at 37 °C and 7% CO_2.

2.3. Preparation of nanoparticles

Preparation of PLGA nanoparticles (PN) was done by o/w emulsion solvent evaporation method (Kumar et al., 2004). Briefly, 50 mg of PLGA was dissolved in 5 ml of ethyl acetate (organic phase). The organic phase was added drop wise to a 5 ml solution of 2% of PVA in purified water (Purelab Flex 4, Elga Labwater, High Wycombe, UK). The resultant emulsion was then homogenized using Ultra-turrax homogenizer (IKA-T25, IKA Werke, Staufen, Germany) with 18 G dispersing stainless steel element at a constant speed of 14,000 rcf for 10 min. Water was added to facilitate organic solvent evaporation (see Graphical Abstract). Sorafenib-loaded PLGA nanoparticles (PNS) were prepared by the same method, except that SFB was dissolved in THF:EtOH (4:1) and was mixed with PLGA solution in ethyl acetate. The prepared nanoparticles were washed three times with purified water followed by centrifugation (14000 rcf for 10 min) for each washing step. Finally, nanoparticles were re-suspended in purified water.

2.4. Surface modification of nanoparticles

Surface modification of nanoparticles was carried out using EDC and NHS coupling reaction with a primary amine at the 3′prime end of Apt. Nanoparticles were washed three times with purified water followed by centrifugation and finally re-suspended in MES buffer (pH 5.5). Nanoparticles were then treated with 400 mM EDC and 200 mM NHS for 30 min for surface activation. The particles were incubated with Apt at a nanoparticle:Apt ratio of 1:12. This resulted in the reaction of the primary amine of Apt with EDC/NHS activated nanoparticles. After 2 h of incubation, washing was done with purified water and nanoparticles were re-suspended in purified water (see Graphical Abstract). The modified particles were stored at

4 °C until further use.

2.5. Encapsulation efficiency and in vitro release profile

PNS were centrifuged (Eppendorf centrifuge 5418, Eppendorf, Germany) at 14,000 rcf for 10 min. The supernatant was removed and the pellet was dissolved in DMSO to extract the drug from the nanoparticles. Samples were analyzed by UV spectrophotometry (UV mini 1240, Shimadzu, Japan) at 265 nm. A calibration curve was recorded with known concentrations of the drug. The solvent background was recorded from nanoparticles without drug and encapsulation efficiency was calculated using the following equation:

$$EE(\%) = \frac{Amount\ \ of\ \ drug\ \ loaded}{Amount\ \ of\ \ drug\ \ added} * 100$$

Release profile of SFB from aptamer modified PLGA nanoparticles was evaluated in PBS (pH 7.4) and in PBS (pH 5) adjusted with 0.1 N HCl to mimic the lysosomal pH. Both contained 1% v/v Tween 80.1 ml of nanoparticle suspension was washed thrice with PBS, followed by centrifugation at 14,500 rcf for 10 min. The pellet was re-suspended in 1 ml PBS with 1% Tween 80 and placed in an orbital shaker, KS4000 IC (IKA Werke, Staufen, Germany) at 150 rpm and 37 ± 0.5 °C. The samples were removed after designated time intervals, after centrifugation, the pellets were re-suspended in 1 ml PBS/HCl and returned to the shaker. After defined time intervals, pellets were dissolved in 1 ml DMSO and analyzed by UV spectrophotometer (UV mini 1240, Shimadzu, Japan) at 265 nm. The vehicle background was then subtracted by measuring the pellet of PLGA nanoparticles, without SFB, prepared under the same condition.

2.6. Aptamer coupling

Fluorescence of Cyn 5 labeled Apt was quantified in nanoparticles to assess the binding of Apt with nanoparticles. For this, freshly prepared surface modified nanoparticles were washed and fluorescence of the supernatant and the pellet was quantified using a Fluostar Optima plate reader (BMG Labtech, Offenburg, Germany) at λ_{ex} 630 nm and λ_{em} 670 nm.

2.7. FTIR spectroscopy

The assessment of coupling of Apt with nanoparticles by Fourier transform infrared spectroscopy (FTIR) was done by single reflection diamond ATR module FTIR (Alpha-P, Bruker Instruments, Massachusetts, USA). Freeze dried nanoparticles were loaded onto ATR platinum diamond crystal. Back correction was done in the absence of any sample. The average of 21 scans at spectral resolution of 2 cm^{-1} was taken automatically to obtain each spectrum. The spectrum was collected at a range between 4000 cm^{-1} and 400 cm^{-1} and was expressed as % transmittance.

2.8. Elemental analysis

PLGA and PVA molecules lack nitrogen in their atomic structure. However, the Apt contains nitrogen as a part of nucleotide bases. This fact was used to analyse the presence or absence of Apt in formulations by elemental analysis. Freeze dried samples were taken in aluminium crucibles, weighed and loaded into the elemental analyzer combustion

chamber (VarioMicro Cube, Elementar Analysensyteme, GmbH, Langenselbold, Germany). Percentage of carbon, hydrogen and nitrogen was obtained and averages of three independent formulations were considered.

2.9. Particle size and zeta potential

The size distribution of the formulations was measured by dynamic light scattering (DLS) using Zetasizer Nano ZS (Malvern Instruments, Malvern, UK). Samples were diluted with purified water in a ratio of 1:50 and were analyzed. Before the measurement, the sample temperature was equilibrated to 25 °C. All the measurements were done independently in triplicates and the sub runs were adjusted by the instrument automatically. Size distribution was evaluated by intensity distribution. Zeta potential was assessed by laser doppler velocimetry (LDV) using the same instrument at conductivity of < 100 µS/cm.

2.10. Atomic force microscopy (AFM)

To study the morphology of the nanoparticles, samples were diluted (1:100) with purified water and were analyzed using atomic force microscopy (Nano Wizard, JPK Instruments, Berlin, Germany). Samples were pipette onto silicon wafers. After 10 min, the liquid was aspirated and was let dry for 5 min. After drying, samples were analyzed by aluminium coated silicon nitride cantilever (HQ: NSC14AL/BS, Mikromasch, Tallinn, Estonia) at a frequency of 148 kHz and a force constant of 5 N/m. Scan speed was adjusted between 0.5 and 1.5 Hz. The surface roughness was measured automatically by JPK data processing software and was mentioned in the form of root mean square average (RMS Rq) values (Nanda et al., 1998; Sitterberg et al., 2010; Mohebi et al., 2017).

2.11. Cell viability assay

Cell viability and IC_{50} values were evaluatedusing3-(4,5-dimethylthiazol-2-yl)-2,5-diphenyltetrazolium bromide (MTT) assay. 10,000 MDA-MB-231 cells/well (0.35 cm^2) were seeded in a 96-well plate and were incubated for 24 h. The cells were then treated with different concentrations of SFB-loaded nanoparticles. After 5 h of incubation, the medium was removed and replaced with fresh medium and incubated further. After 12 h, the medium was removed and replaced with 2 mg/ml MTT reagent containing medium and incubated for 4 h. The resultant formazan crystals were dissolved using DMSO and absorbance was measured in a FluoStar Optima plate reader at 570 nm. The experiment was repeated three times and the percentage cell viability was calculated. IC_{50} values were calculated by the concentration of nanoparticles showing 50% of the cell survival.

2.12. Internalization pathway

MDA-MB-231 cells were seeded into 96 well plates in a similar manner as for the viability experiments. After 24 h, the cells were incubated with either filipin III (6 µg/ml) or chlorpromazine (6 µg/ml) for 2 h. Cells were then treated with the formulations containing 1.5 µM SFB. After 5 h of incubation, the medium was removed and replaced with fresh medium. The cells were subsequently incubated for 12 h and the cell viability was determined by MTT assay as described above.

2.13. Apoptosis assay

MDA-MB-231 cells were cultured on sterile cover slips in 24well plates at a seeding density of50,000 cells per well (1.8 cm^2) for 24 h. Cells were washed thrice with cold PBS buffer (pH 7.4). 500 µl of different formulations were added to the wells. After 12 h, cells were washed again with PBS and fixed using 4% paraformaldehyde for 15 min. Cells were counterstained using DAPI (0.1 mg/ml) solution for 20 min. Washing was performed with PBS and cells were examined using a fluorescence microscope (CKX53, Olympus, Tokyo, Japan).

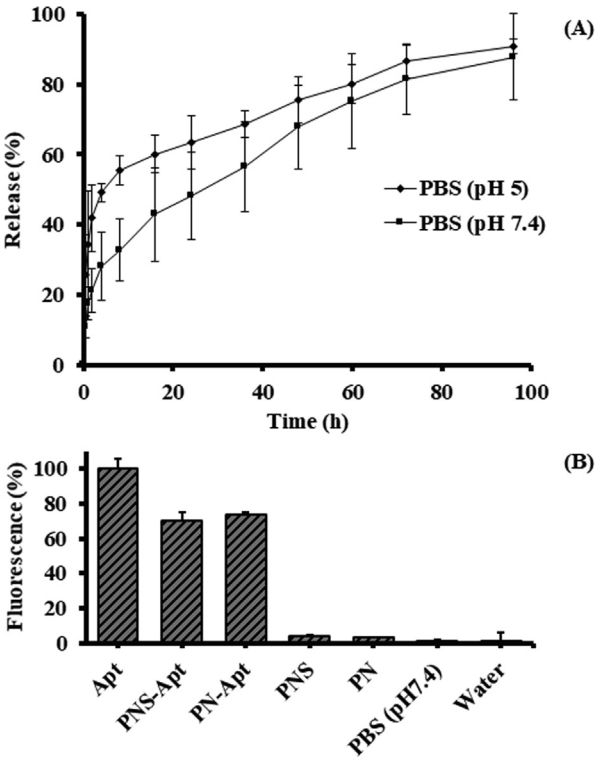

Fig. 1. A. Release profile of sorafenib tosylate from aptamer modified PLGA nanoparticles. B. Fluorescence analysis of cyanine 5-Apt at $\lambda_{ex}/\lambda_{em}$ 630/670 nm on sorafenib tosylate-loaded nanoparticles (PNS) and blank nanoparticles (PN), the fluorescence of Cyn 5 of pure Apt was considered as a reference. All experiments were performed thrice (n = 3) and the results are the averages of these experiments.

Table 1
Size (by dynamic light scattering and atomic force microscopy) and zeta potential of nanoparticles. Three independent samples (n = 3) were considered for the measurements and the results are the averages of these measurements.

Formulation	Size ± SD (nm)		Zeta Potential ± SD (mV)	PdI ± SD
	DLS	AFM		
PN	179.7 ± 5.9	254.9 ± 16.2	−16.2 ± 0.7	0.19 ± 0.02
PNS	185.1 ± 10.3	259.0 ± 16.8	−14.0 ± 0.5	0.21 ± 0.05
PN-Apt	204.9 ± 12.5	263.0 ± 28.5	−18.0 ± 1.8	0.24 ± 0.03
PNS-Apt	222.3 ± 9.9	262.3 ± 19.0	−16.7 ± 2.5	0.22 ± 0.07

2.14. Ex vivo hemolysis assay

To determine the compatibility of the formulations with blood, human erythrocytes were isolated from fresh blood as described previously (Pinnapireddy et al., 2017). Briefly, erythrocytes were obtained by centrifugation of fresh blood in tubes containing EDTA. The pellet was washed three times with PBS buffer (pH 7.4) and diluted to 1:50 with PBS. The erythrocytes were incubated together with the formulations (equivalent to 1.5 µM SFB) in v-bottom microtitre plates (1 h, 37 °C) and placed in an orbital shaker. The plates were centrifuged and the absorbance of the collected supernatant was determined at 540 nm in a FluoStar Optima plate reader. As controls, saline (NaCl 0.9%), 1% Triton X-100 and blood were used.

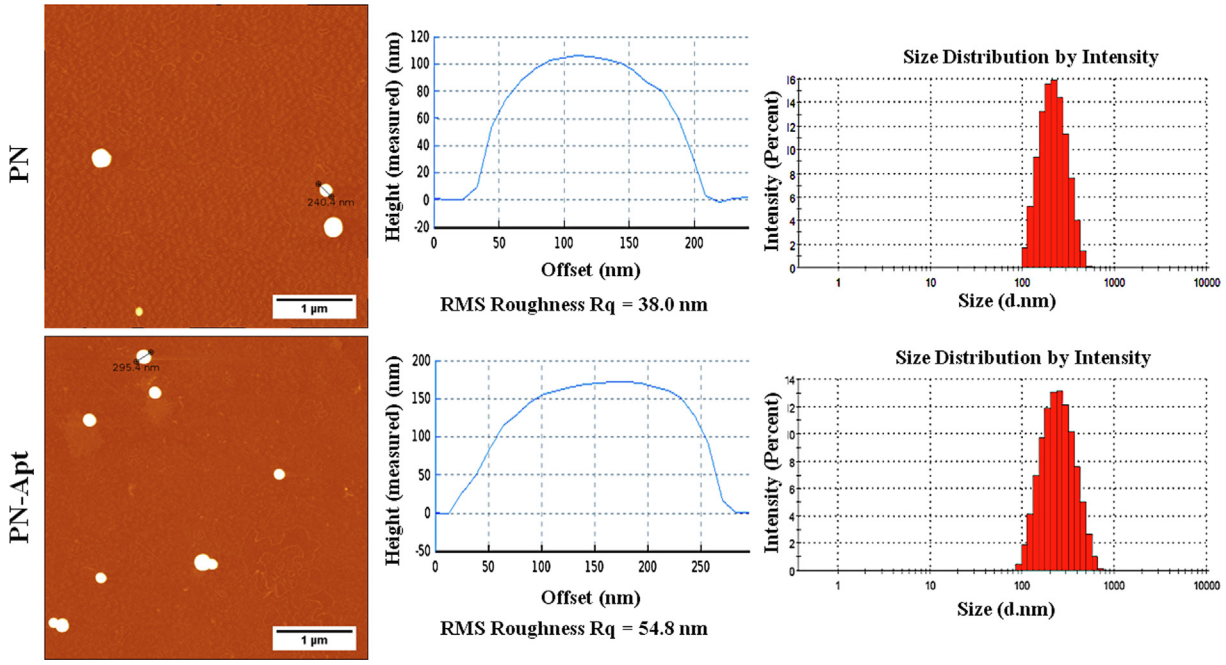

Fig. 2. AFM images (height) of nanoparticles with cross sectional profile (surface roughness; Rq) along the identified line (graph). Images on the right side depict the size histogram (dynamic light scattering) of the nanoparticles. Scale bar represents 1 µm.

2.15. Reactive oxygen species assessment

Determination of ROS production was done using 2′,7′-dichlorodihydrofluorescein diacetate (carboxy-H_2DCFDA) conversion into 2′,7′-dichlorofluorescein (DCF) as previously reported (Duse et al., 2018). Briefly, MDA-MB-231 cells grown in 96 well plates for 24 h were washed (PBS buffer; pH 7.4) and incubated with phenol red-free medium containing 25 µM of carboxy-H_2DCFDA for 45 min. The cells were subsequently washed twice with PBS. Cells were then treated with formulations containing 1.0 µM and 1.5 µM of SFB. After 1 h, cells were washed again with PBS and lysed using lysis reagent (Promega, Mannheim, Germany).The fluorescence was observed at λ_{ex} 485 nm/ λ_{em} 520 nm using a FluoStar Optima plate reader.

2.16. Metastatic progression

Inhibition of cell migration and metastasis was evaluated by wound healing assay. MDA-MB-231cells were seeded in 24 well plate. After 24 h, cells were treated with formulations containing 5 µM SFB for 2 h in serum-free medium. A scratch was made with a 200 µl pipette tip. Cells were then washed twice with ice-cold PBS (pH 7.4) and fresh medium was added. Wound closure was observed using an inverted microscope (CKX53, Olympus, Tokyo, Japan) at different time intervals. Cell migration and percentage wound healing were also calculated using SketchAndCalcTM® along with Gimp2.10.10® application software measuring the distance between wound closures.

2.17. Cellular uptake

For cellular uptake studies, MDA-MB-231 cells were cultured on sterile cover slips in 12-well plates at a seeding density of 90,000 cells per well (3.5 cm^2). After 24 h, the supernatant was removed and washed three times with PBS (pH 7.4). Cells were incubated for either 30 min or 2 h with different formulations. After washing with PBS cells were fixed with 4% paraformaldehyde for 20 min. Cell nucleus was then counterstained with DAPI (0.1 µg/ml) for 15 min in the dark. Cells were washed and the cover slips were mounted on to glass slides and with FluorSave (Calbiochem Corp, La Jolla, USA). Uptake analysis was performed using a confocal laser-scanning microscope (LSM700, Carl Zeiss, Jena, Germany).

2.18. Statistical analysis

All experiments were performed in triplicates and the values were presented as mean ± standard deviation unless otherwise stated. One way ANOVA was performed to identify statistically significant differences between the groups using GraphPad Prism software. The probability values < 0.05 were considered significant. Statistical differences were denoted as "*" $p < 0.05$, "**" $p < 0.01$ and "***" $p < 0.001$.

3. Results and discussion

3.1. Preparation of nanoparticles

Size plays an important role in cellular uptake of the nanoparticles (Prabha et al., 2002). Therefore, the concentration of PLGA and PVA used for the preparation of nanoparticles by solvent evaporation was adjusted in preliminary experiments. Several solvents were screened and we found that the particle size was at its lowest (data not shown) using ethyl acetate with drug solution in THF:EtOH (4:1). The homogenization step further decreased particle size. Furthermore, homogenization along with constant stirring and addition of water facilitated the evaporation of organic phase (see Graphical Abstract). The formed nanoparticles were then washed and used for further studies discussed in following sections.

3.2. Encapsulation efficiency and in vitro release profile

A challenging issue regarding the preparation of nanoparticles is encapsulation of drug. Encapsulation efficiency of SFB in nanoparticles was 85.0 ± 2%. Since SFB was insoluble in water, a majority of it was encapsulated in the PLGA matrix. Once incorporated, the amount of SFB released from PNS was calculated in percentage and data is shown in Fig. 1A. It is evident from the results that more than 50% drug was released from PNS-Apt in PBS (pH 7.4) and more than 60% in PBS (pH

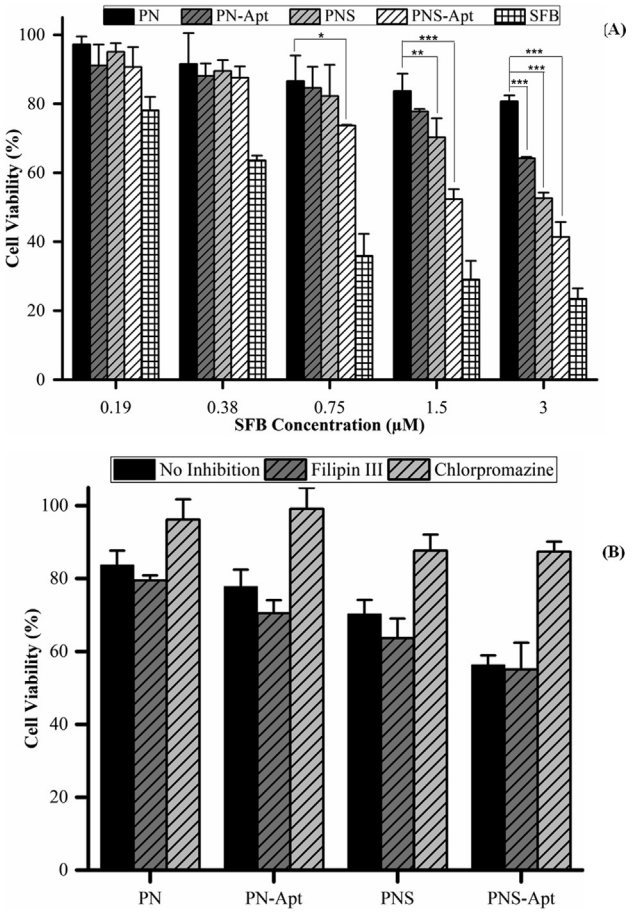

Fig. 3. A. Cell viability assay; B. Pathway analysis of PLGA nanoparticles (PN), surface modified PLGA nanoparticles (PN-Apt), SFB-loaded PLGA nanoparticles (PNS) and surface modified SFB-loaded PLGA nanoparticles (PNS-Apt). Each formulation was equivalent to 1.5 μM SFB concentration in nanoparticles. All experiments were performed thrice (n = 3) and the results are the averages of these experiments. Statistical differences (Fig. 3A) are denoted as "*" $p < 0.05$, "**"$p < 0.01$ and "***" $p < 0.001$.

5) within the first 24 h. 87.1 ± 6.2% SFB for PBS (pH 7.4) and 92.1 ± 2.4 SFB for PBS (pH 5) were subsequently released until 96 h. The initial burst release was due to the presence of SFB on the surface of the nanoparticles. The subsequent release was due to drug entrapment inside nanoscale formulations. This second release phase in case of PBS could be due to the diffusion from the pores of non-degraded PLGA matrix as reported previously (Prakapenka et al., 2017; Jonderian and Maalouf, 2016).

3.3. Aptamer coupling

Binding of Apt on the surface of nanoparticles was evaluated by fluorescence analysis of Cyn 5. Fluorescence quantification at λ_{ex} 630 nm and λ_{em} 670 nm confirmed the attachment of Cyn 5 labeled Apt to the nanoparticle surface. The results showed that 73.9 ± 4 and 70.6 ± 5 percent of Apt was bound on the surface of PN and PNS respectively (Fig. 1B).

3.4. FTIR spectroscopy

FITR was used to confirm the presence of SFB and Apt in nanoparticle formulations (supplementary data). PN showed a characteristic peak of carboxylic acid (from PLGA) at 1751 cm^{-1}. The presence of SFB (in PNS) showed peaks of alkene stretching at 1503 cm^{-1}. On the other hand, in the spectrum of PN-Apt and PNS-Apt conjugated acid stretching at 1703 cm^{-1} along with imine peaks at 1650 cm^{-1} were observed. These results showed the presence of SFB in PNS as well as in PNS-Apt. Moreover, peaks of imine showed the coupling of Apt with PLGA in nanoparticles in PN-Apt and PNS-Apt formulations. This confirms the successful EDC/NHS surface coupling reaction.

3.5. Elemental analysis

Nucleotide bases of Apt contain nitrogen. Therefore, the assessment of presence of Apt can also be done by elemental analysis. Freeze dried nanoparticles were directly subjected to combustion in the presence of oxygen. Percentages of carbon, hydrogen and nitrogen were calculated. PNS showed 0.25 ± 0.06% nitrogen due to presence of SFB as compared to 0% in case of PN. On the other hand, PN-Apt and PNS-Apt showed 1.16 ± 0.45% and 0.51 ± 0.25% nitrogen content (with respect to carbon and hydrogen percentages), respectively. This confirmed the results obtained from the FTIR analysis.

3.6. Particle size and zeta potential

Solvent evaporation method used to prepare nanoparticles. Preliminary experiments were performed to optimize the concentration of PVA, homogenization speed and drug loading. Optimized formulations were then assessed for size (hydrodynamic diameter as a function of intensity) and zeta potential. The size distribution (Polydispersity Index; PdI) was found to be 0.19 ± 0.02 in case of PN. It was obvious that particle size increased by incorporating the drug into nanoparticles with a slight increase in PdI to 0.21 ± 0.05 (Table 1). On the other hand, the presence of Apt also changed the size of the nanoparticles. Similar increase in diameter, after attachment of Apt on the surfaces of nanoparticles, was also reported earlier (Farokhzad et al., 2006; Guo et al., 2017). The incorporation of SFB as well as the presence of Apt also influenced the zeta potential. Chemical modification of surfaces of nanoparticles required multiple washings and treatments with EDC/NHS coupling agents. This resulted in an increase in size and zeta potential of the nanoparticles. Multiple washing and EDC/NHS treatment also influenced the PdI.

3.7. Atomic force microscopy

Morphological characterization was done using an atomic force microscope (AFM). AFM analysis revealed spherical shaped particles among all formulations (Fig. 2). The coupling of Apt resulted in an increase in the size and size distribution of the modified particles. Surface roughness (by RMS; Rq) of the nanoparticles was also calculated with 38.0 ± 14.8 nm for PN and 54.8 ± 7.1 nm in case of PN-Apt. This increase in Rq value represented surface modification in case of PN-Apt. More the surface roughness more will be the wettability of the nanoparticles and thus will affect nanoparticle-cell interaction (Nanda et al., 1998; Sitterberg et al., 2010; Marrese et al., 2017).

3.8. Cell viability assay

MTT assay was performed to assess the cell viability. Cell viability was dose-dependent, increasing with decreasing the nanoparticle concentration. Maximum viability for PNS-Apt was achieved with 0.19 μM SFB. IC_{50} values were 0.5 μM, 1.5 μM, 2.0 μM, 4.5 μM and 6.9 μM for SFB, PNS-Apt, PNS, PN-Apt and PN, respectively. In case of formulations without SFB, an equivalent nanoparticle amount was considered.PN showed a cell viability of more than 80% as shown in Fig. 4A. This depicted the safety of formulations, in the absence of Apt or SFB. The presence of Apt along with SFB decreased cell viability significantly. This decrease indicated the interaction between anti-ErbB3-Apt modified particles and cells on one hand and anti-proliferation effect of SFB itself on the other hand. Therefore, this combination of anti-ErbB3-Apt and drug exhibited a synergistic effect thereby

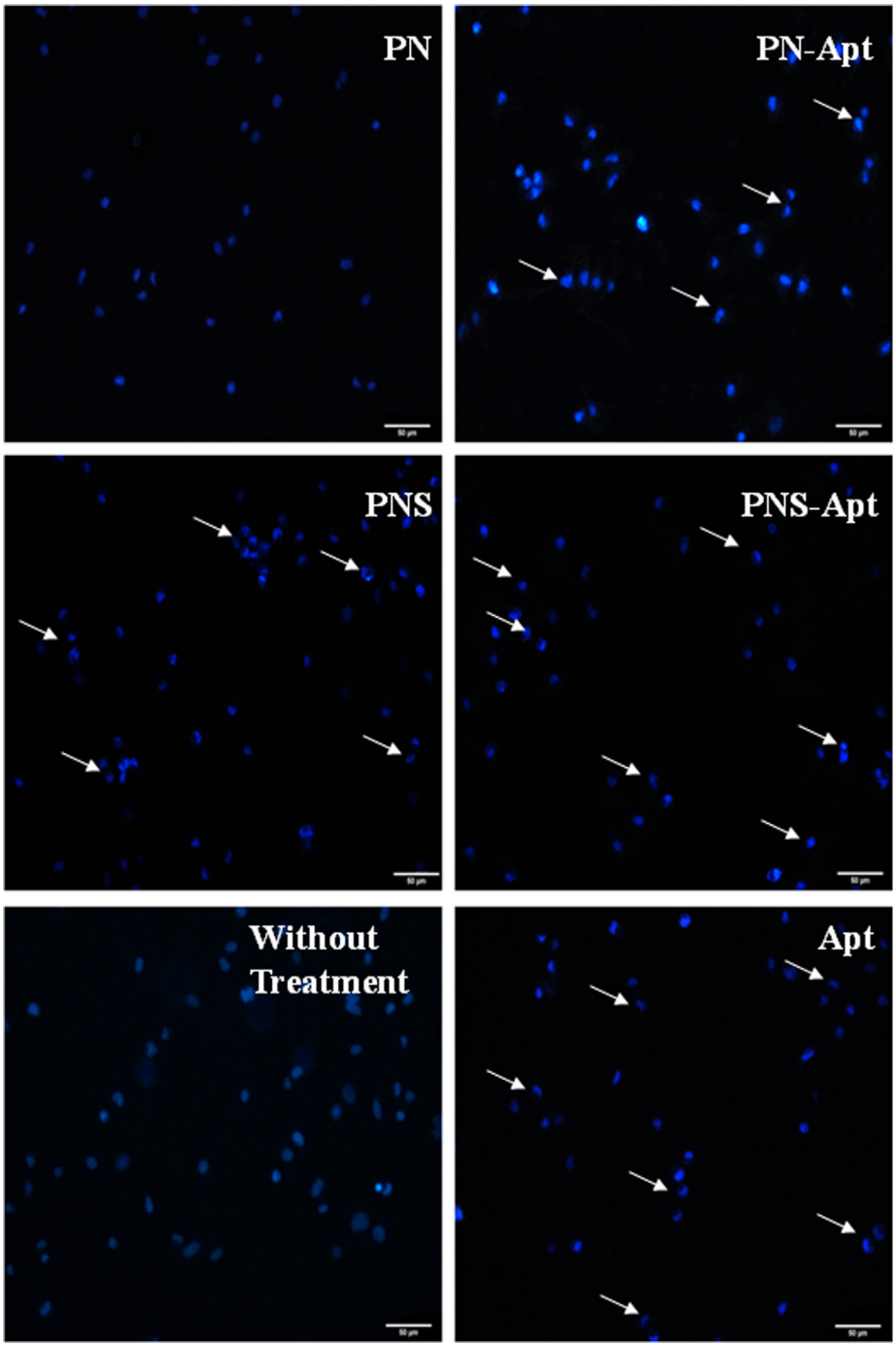

Fig. 4. Apoptotic assay by DAPI staining; Arrows localize the formation of apoptotic bodies (nuclear condensation and chromatin degradation): PLGA nanoparticles (PN), surface modified PLGA nanoparticles (PN-Apt), SFB-loaded PLGA nanoparticles (PNS-Apt) and surface modified SFB-loaded PLGA nanoparticles (PNS-Apt).

addressing the problem of resistance towards SFB (Bijman et al., 2009; Xu et al., 1999; Göstring et al., 2012; Powell et al., 2017).

3.9. Internalization pathway

To examine the mechanism of nanoparticle internalization into MDA-MD-231 cells, different endocytosis pathways were used. Chlorpromazine and Filipin III were used to suppress the clathrin and the caveolae mediated endocytosis, respectively. It was evident from the results that cells, pre-treated with chlorpromazine, showed increased cell viability as compared to control group and Filipin III group (Fig. 3B). Chlorpromazine blocks clathrin dependent internalization pathway of receptor tyrosine kinase (Guo et al., 2017; Broecker-Preuss et al., 2015; Zhai et al., 2014). The presence of chlorpromazine resulted in the blockade of nanoparticle internalization. This was evident from the increased cell viability in chlorpromazine treated cells. On the other hand, Filipin III blocks caveolae-mediated endocytosis. A decreased cell viability in its presence further endorsed that the clathrin dependent pathway as a possible mechanism of nanoparticle internalization.

3.10. Apoptosis assay

The mechanism of cell death was evaluated by DAPI staining. DAPI is a nuclear stain, which binds to double-stranded DNA. It can be used

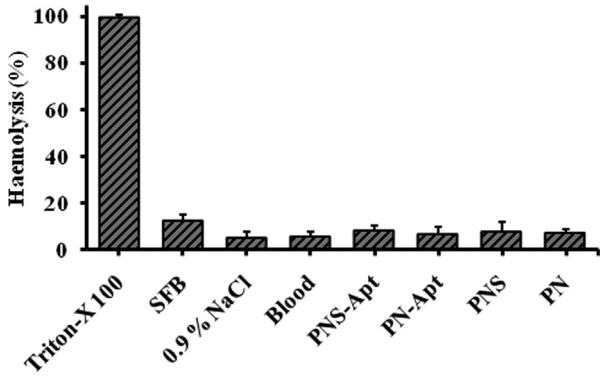

Fig. 5. Hemolysis assay of the PLGA nanoparticles (PN), surface modified PLGA nanoparticles (PN-Apt), SFB-loaded PLGA nanoparticle (PNS-Apt) and surface modified SFB-loaded PLGA nanoparticle (PNS-Apt). 1% Triton-X 100, 0.9% NaCl and blood were used as controls. All experiments were performed thrice (n = 3) and the results are the averages of these experiments.

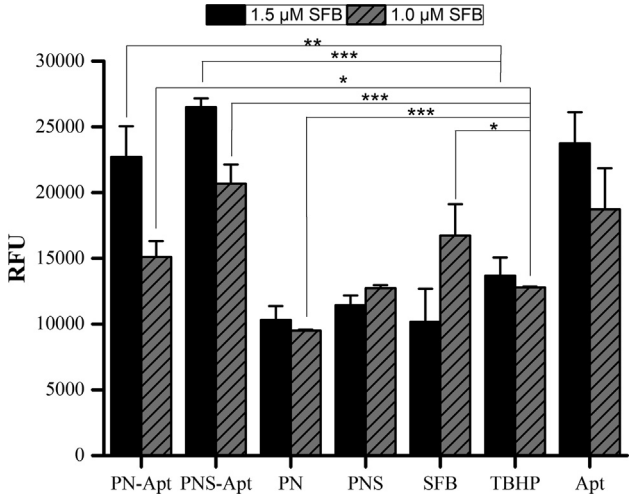

Fig. 6. ROS production after treatment with PLGA nanoparticles (PN), surface modified PLGA nanoparticles (PN-Apt), SFB-loaded PLGA nanoparticle (PNS-Apt) and surface modified SFB-loaded PLGA nanoparticle (PNS-Apt). Tert-Butyl hydroperoxide (TBHP) was used as positive control. Statistical differences are denoted as "*" $p < 0.05$, "**"$p < 0.01$ and "***" $p < 0.001$.

for the detection of chromatin or nuclear condensation and degradation. DAPI staining is frequently used for the localization of apoptotic bodies which result ultimately in the death of cells (Xiao et al., 2017; Nicolete et al., 2011). When cells were treated with different formulations, significant damage and apoptotic bodies' formation was observed (localized by arrows in Fig. 4). Cell shrinkage and chromatin, as well as nuclear condensation, were observed in case of cells treated with Apt and SFB. On the other hand, untreated cells (blank) show no clear evidence of apoptotic bodies' formation. The presence of Apt and SFB were therefore responsible for the apoptosis leading to cell death. These results were also in agreement with cell viability assay, showing more apoptotic bodies in the presence of both Apt and SFB (higher cytotoxicity) as compared to other formulations.

3.11. Ex vivo hemolysis assay

Compatibility of formulations with erythrocytes was evaluated by hemolysis assay. This assay determines the release of hemoglobin from erythrocytes after exposure to nanoparticles. Percentage of oxyhemoglobin formed after the reaction of released hemoglobin with atmospheric oxygen can be determined spectroscopically. Hemolytic potential among all formulations was less than 15% indicating a good

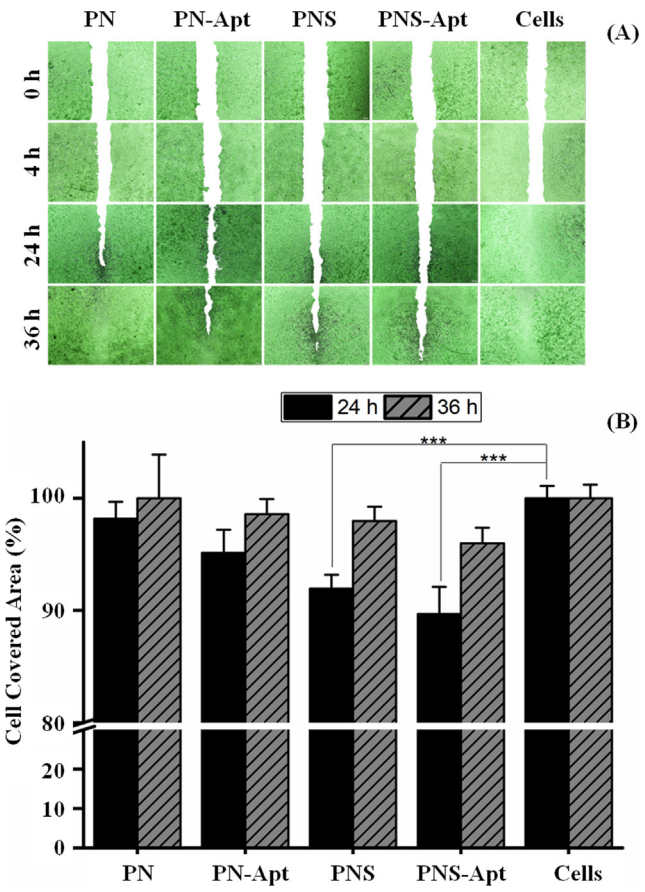

Fig. 7. Effect of formulations on cell growth; Scratching was perfromed using a 200 µl pipette tip. A. Metastatic progression by scratch test.B.Time dependent cell migration under the influence of PLGA nanoparticles (PN), surface modified PLGA nanoparticles (PN-Apt), SFB-loaded PLGA nanoparticles (PNS-Apt) and surface modified SFB-loaded PLGA nanoparticles (PNS-Apt). Statistical differences are denoted as "*" $p < 0.05$, "**"$p < 0.01$ and "***" $p < 0.001$.

haemocompatibility profile (Fig. 5). Maximum hemolysis of 13 ± 2.1% was observed in case of pure drug. From the results, it can be concluded that the presence of Apt and SFB did not affect the normal physiology of erythrocytes, thereby rendering the formulations suitable for i.v. administration.

3.12. Reactive oxygen species assessment

Reactive oxygen species (ROS) can convert carboxy-H_2DCFDA into DCF and are responsible for cell death in higher concentrations. Upon treatment of the cells with different concentration of nanoparticles (equivalent to 1.0 µM and 1.5 µM SFB i.e. $\leq IC_{50}$ from MTT assay), a significant dose-dependent ROS production was noticed (Fig. 6). SFB formulations showed variable results due to a decrease in cell viability with increasing concentrations of SFB. This was in accordance with the previously reported results i.e. the presence of any aptamer and drug together increases the production of ROS (Sauer et al., 2001; Sasaki et al., 2013; Son et al., 2011).

3.13. Metastatic progression

Cell progression, migration and inhibition of apoptosis are all associated with the progression of cancer. ErbB3 is one of the responsible receptor involved in these progressions (Belleudi et al., 2012; Roepstorff et al., 2008; Sasaki et al., 2013). On the other hand, SFB has also been reported to inhibit metastasis (Yoshida et al., 2017; Jiang et al., 2018). Therefore, we performed a wound healing assay to assess

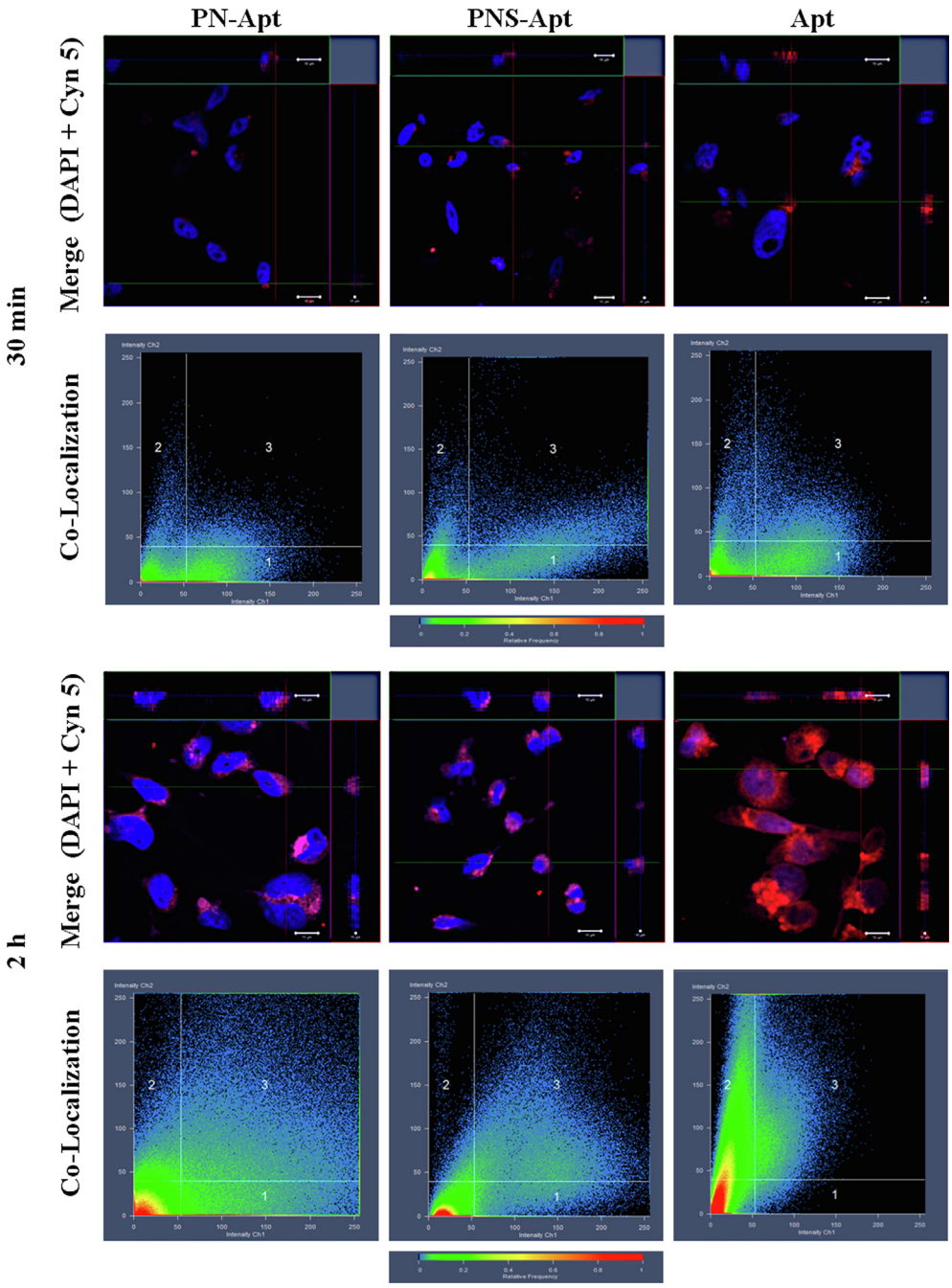

Fig. 8. Cellular uptake of Cyn 5 labeled nanoparticles (red) after: A. 30 min and B. 2 h; micrographs are represented in the form of z-stack images to represent the presence of aptamer-functionalized nanoparticles near nucleus (blue; DAPI staining). Co-localization is shown in intensity plots mapping the intensity of Cyn 5 (aptamer) and DAPI (cell nucleus) of surface modified PLGA nanoparticles (PN-Apt), SFB-loaded PLGA nanoparticle (PNS-Apt) and aptamer treated cells (Apt). (For interpretation of the references to colour in this figure legend, the reader is referred to the web version of this article.)

the inhibition of metastasis. Presence of Apt and SFB blocked progression and wound healing significantly as compared to untreated cells up to 24 h ($p < 0.001$). The percentage of wound healing was in decreasing order i.e. untreated cells > PN > PN-Apt > PNS > PNS-Apt (100%, 98%, 95%, 91% and 89% respectively). However, after 36 h more than 95% area was covered by the cells in all treatment cases. Nevertheless, Apt and SFB blocked wound healing but in the presence of only one of these or in the absence of both, cell migration rate was higher. From these findings, it was clear that presence of Apt and SFB have a synergistic effect in blocking metastatic progression (see Fig. 7).

3.14. Cellular uptake

Cyanine 5 was attached to the 5′ end of Apt as a fluorophore. Detection of its fluorescence was used to visualize the uptake of the nanoparticles. Cells were treated for two different time points (30 min and 2 h). After 30 min of the treatment of cells, most of the nanoparticles accumulated in cytoplasm near the cell membrane. On the other hand, upon incubation with the nanoparticles for 2 h, fluorescence was observed mostly near the nucleus. This was also confirmed by z-stack images as shown in Fig. 8.The intensity plot for co-localization shows the intensity of DAPI (cell nucleus) on the x-axis and Cyn 5 (aptamer) on the y-axis. Co-localization coefficient was measured by

ZEN software (Carl Zeiss). This ranges from 0 to 1, where 0 indicates no co-localization and 1 indicates 100 percent co-localization.

Clathrin dependent internalization and endocytosis was found to be responsible for the transfer of nanoparticles from cell membrane to nucleus. ErbB3 receptors are also internalized by this mechanism (Adilakshmi et al., 2011). Time dependent locations of nanoparticles were due to this mechanism of transport. Increased cellular toxicity was observed due to binding of the nanoparticles with these receptors (Mahmoud et al., 2018). The z-stack images showed the presence of Cyn 5 labeled aptamer in nuclear region. Co-localizations were differential, showing co-localization coefficients less than 0.4 in case of 30 min incubation time with nanoparticles. This represented the location of nanoparticles in cytoplasm away from DAPI channel (nucleus). However, for 2 h treatment time, co-localization coefficient was above 0.7, representing nearly the same location of DAPI and Cyn 5 suggesting that the nanoparticles were closer to the nucleus. Based on these findings, Apt modified nanoparticles may be used as a carrier for targeted drug delivery to the cytoplasm of cells rich in ErbB3 receptors. The presence of a drug together with aptamer would result in specific effects to arrest the growth or even destroy the cells.

4. Conclusion

The current study was designed to improve the efficiency of SFB cancer therapy using SFB-loaded PLGA nanoparticles coupled with anti-ErbB3-aptamer. The main aim was to formulate surface modified SFB nanoparticles, so that generalized toxicity of non-specific chemotherapeutic drug entity may be reduced. Physicochemical analysis of the formulations revealed a nanoscaled profile suitable for cellular internalization. Morphological analysis by AFM further supported these results and showed an optimal surface roughness profile for cell surface interactions. Another positive impact of the combination was the synergism of Apt and SFB. PNS-Apt showed maximum cytotoxicity compared to other formulations due to the presence of Apt and SFB together. Dose-dependent toxicity was demonstrated using the cell viability assay. Moreover, time-dependent nanoparticles delivery, to the cytoplasm and subsequently to the nuclear membrane, was observed by CLSM visualization. Increasing the incubation time resulted in higher cytotoxicity. Higher ROS production was observed in the presence of both Apt and SFB. *Ex vivo* hemolysis studies demonstrated the hemocompatibility of the nanoparticles. The metastatic inhibition potential of the nanoparticles, especially those with Apt and SFB was evident from the scratch test. With the aim of developing a formulation suitable for therapy of SFB resistant tumors, we would direct out efforts towards the *in vivo* assessment of these nanoparticles.

CRediT authorship contribution statement

Muhammad Yasir Ali: Investigation, Validation, Visualization, Formal analysis. **Imran Tariq:** Investigation. **Sajid Ali:** Investigation. **Muhammad Umair Amin:** Investigation. **Konrad Engelhardt:** Investigation. **Shashank Reddy Pinnapireddy:** Methodology. **Lili Duse:** Investigation. **Jens Schäfer:** Methodology, Supervision. **Udo Bakowsky:** Resources, Supervision, Project administration.

Declaration of Competing Interest

The authors declare that they have no known competing financial interests or personal relationships that could have appeared to influence the work reported in this paper.

Acknowledgments

Authors would like to extend thanks to DAAD Germany, HEC Pakistan, GC University Faisalabad and overseas scholarship committee University of the Punjab, Pakistan for providing the support and funding, Dr. Brüßler and Dr. Jedelska for fruitful discussions during research and Mrs. Mohr for technical assistance in cell culture experiments.

Appendix A. Supplementary material

Supplementary data to this article can be found online at https://doi.org/10.1016/j.ijpharm.2019.118961.

References

Farokhzad, O.C., Cheng, J., Teply, B.A., Sherifi, I., Jon, S., Kantoff, P.W., Richie, J.P., Langer, R., 2006. Targeted nanoparticle-aptamer bioconjugates for cancer chemotherapy in vivo. Proc. Natl. Acad. Sci. 103, 6315–6320.
Aravind, A., Varghese, S.H., Veeranarayanan, S., Mathew, A., Nagaoka, Y., Iwai, S., Fukuda, T., Hasumura, T., Yoshida, Y., Maekawa, T., 2012. Aptamer-labeled PLGA nanoparticles for targeting cancer cells. Cancer Nanotechnol. 3, 1.
Muthu, M.S., Singh, S., 2009. Targeted nanomedicines: effective treatment modalities for cancer. AIDS Brain Disorders.
Dinarvand, R., Sepehri, N., Manoochehri, S., Rouhani, H., Atyabi, F., 2011. Polylactide-co-glycolide nanoparticles for controlled delivery of anticancer agents. Int. J. Nanomed. 6, 877.
Plourde, K., Derbali, R.M., Desrosiers, A., Dubath, C., Vallée-Bélisle, A., Leblond, J., 2017. Aptamer-based liposomes improve specific drug loading and release. J. Control. Release 251, 82–91.
Wu, X., Chen, J., Wu, M., Zhao, J.X., 2015. Aptamers: active targeting ligands for cancer diagnosis and therapy. Theranostics 5, 322.
Ozalp, V.C., Eyidogan, F., Oktem, H.A., 2011. Aptamer-gated nanoparticles for smart drug delivery. Pharmaceuticals 4, 1137–1157.
McKeague, M., DeRosa, M.C., 2012. Challenges and opportunities for small molecule aptamer development. J. Nucl. Acids 2012.
Jo, H., Ban, C., 2016. Aptamer–nanoparticle complexes as powerful diagnostic and therapeutic tools. Exp. Mol. Med. 48, e230.
Szymanska, M., Fosdahl, A.M., Raiborg, C., Dietrich, M., Liestøl, K., Stang, E., Bertelsen, V., 2016. Interaction with epsin 1 regulates the constitutive clathrin-dependent internalization of ErbB3, Biochimica et Biophysica Acta (BBA)-Molecular. Cell Res. 1863, 1179–1188.
Belleudi, F., Marra, E., Mazzetta, F., Fattore, L., Giovagnoli, M.R., Mancini, R., Aurisicchio, L., Torrisi, M.R., Ciliberto, G., 2012. Monoclonal antibody-induced ErbB3 receptor internalization and degradation inhibits growth and migration of human melanoma cells. Cell Cycle 11, 1455–1467.
Roepstorff, K., Grøvdal, L., Grandal, M., Lerdrup, M., van Deurs, B., 2008. Endocytic downregulation of ErbB receptors: mechanisms and relevance in cancer. Histochem. Cell Biol. 129, 563–578.
Chen, C.-H.B., Chernis, G.A., Hoang, V.Q., Landgraf, R., 2003. Inhibition of heregulin signaling by an aptamer that preferentially binds to the oligomeric form of human epidermal growth factor receptor-3. Proc. Natl. Acad. Sci. 100, 9226.
Guo, Y., Zhong, T., Duan, X.-C., Zhang, S., Yao, X., Yin, Y.-F., Huang, D., Ren, W., Zhang, Q., Zhang, X., 2017. Improving anti-tumor activity of sorafenib tosylate by lipid-and polymer-coated nanomatrix. Drug Deliv. 24, 270–277.
Broecker-Preuss, M., Müller, S., Britten, M., Worm, K., Schmid, K.W., Mann, K., Fuhrer, D., 2015. Sorafenib inhibits intracellular signaling pathways and induces cell cycle arrest and cell death in thyroid carcinoma cells irrespective of histological origin or BRAF mutational status. BMC Cancer 15, 184.
Zhai, B., Hu, F., Jiang, X., Xu, J., Zhao, D., Liu, B., Pan, S., Dong, X., Tan, G., Wei, Z., 2014. Inhibition of Akt reverses the acquired resistance to sorafenib by switching protective autophagy to autophagic cell death in hepatocellular carcinoma. Mol. Cancer Ther. 13, 1589–1598.
Kumar, M.R., Bakowsky, U., Lehr, C., 2004. Preparation and characterization of cationic PLGA nanospheres as DNA carriers. Biomaterials 25, 1771–1777.
Nanda, K., Sarangi, S., Sahu, S., 1998. Measurement of surface roughness by atomic force microscopy and Rutherford backscattering spectrometry of CdS nanocrystalline films. Appl. Surf. Sci. 133, 293–297.
Sitterberg, J., Özcetin, A., Ehrhardt, C., Bakowsky, U., 2010. Utilising atomic force microscopy for the characterisation of nanoscale drug delivery systems. Eur. J. Pharm. Biopharm. 74, 2–13.
Mohebi, S., Shafiee, H.-A., Ameli, N., 2017. Evaluation of enamel surface roughness after orthodontic bracket debonding with atomic force microscopy. Am. J. Orthod. Dentofac. Orthop. 151, 521–527.
Pinnapireddy, S.R., Duse, L., Akbari, D., Bakowsky, U., 2017. Photo-enhanced delivery of genetic material using curcumin loaded composite nanocarriers. Clinincs in Oncology 2.
Duse, L., Pinnapireddy, S.R., Strehlow, B., Jedelská, J., Bakowsky, U., 2018. Low level LED photodynamic therapy using curcumin loaded tetraether liposomes. Eur. J. Pharm. Biopharm. 126, 233–241.
Prabha, S., Zhou, W.-Z., Panyam, J., Labhasetwar, V., 2002. Size-dependency of nanoparticle-mediated gene transfection: studies with fractionated nanoparticles. Int. J. Pharm. 244, 105–115.
Prakapenka, A.V., Bimonte-Nelson, H.A., Sirianni, R.W., 2017. Engineering poly (lactic-co-glycolic acid)(PLGA) micro-and nano-carriers for Controlled Delivery of 17β-Estradiol. Ann. Biomed. Eng. 45, 1697–1709.
Jonderian, A., Maalouf, R., 2016. Formulation and in vitro interaction of rhodamine-B

loaded PLGA nanoparticles with cardiac myocytes. Front. Pharmacol. 7, 458.
Guo, X., Zhu, X., Gao, J., Liu, D., Dong, C., Jin, X., 2017. PLGA nanoparticles with CD133 aptamers for targeted delivery and sustained release of propranolol to hemangioma. Nanomedicine 12, 2611–2624.
Marrese, M., Guarino, V., Ambrosio, L., 2017. Atomic force microscopy: a powerful tool to address scaffold design in tissue engineering. J. Funct. Biomater. 8, 7.
Bijman, M.N., van Berkel, M.P., Kok, M., Janmaat, M.L., Boven, E., 2009. Inhibition of functional HER family members increases the sensitivity to docetaxel in human ovarian cancer cell lines. Anticancer Drugs 20, 450–460.
Xu, F., Yu, Y., Le, X.-F., Boyer, C., Mills, G.B., Bast, R.C., 1999. The outcome of heregulin-induced activation of ovarian cancer cells depends on the relative levels of HER-2 and HER-3 expression. Clin. Cancer Res. 5, 3653–3660.
Göstring, L., Malm, M., Höidén-Guthenberg, I., Frejd, F.Y., Ståhl, S., Löfblom, J., Gedda, L., 2012. Cellular effects of HER3-specific affibody molecules. PLoS ONE 7, e40023.
Powell, D., Chandra, S., Dodson, K., Shaheen, F., Wiltz, K., Ireland, S., Syed, M., Dash, S., Wiese, T., Mandal, T., 2017. Aptamer-functionalized hybrid nanoparticle for the treatment of breast cancer. Eur. J. Pharm. Biopharm. 114, 108–118.
Xiao, S., Liu, Z., Deng, R., Li, C., Fu, S., Chen, G., Zhang, X., Ke, F., Ke, S., Yu, X., 2017. Aptamer-mediated gene therapy enhanced antitumor activity against human hepatocellular carcinoma in vitro and in vivo. J. Control. Release 258, 130–145.
Nicolete, R., dos Santos, D.F., Faccioli, L.H., 2011. The uptake of PLGA micro or nanoparticles by macrophages provokes distinct in vitro inflammatory response. Int. Immunopharmacol. 11, 1557–1563.
Sauer, H., Wartenberg, M., Hescheler, J., 2001. Reactive oxygen species as intracellular messengers during cell growth and differentiation. Cell. Physiol. Biochem. 11, 173–186.
Sasaki, T., Hiroki, K., Yamashita, Y., 2013. The role of epidermal growth factor receptor in cancer metastasis and microenvironment. Biomed. Res. Int. 2013.
Son, Y., Cheong, Y.-K., Kim, N.-H., Chung, H.-T., Kang, D.G., Pae, H.-O., 2011. Mitogen-activated protein kinases and reactive oxygen species: how can ROS activate MAPK pathways? J. Signal Transduction 2011.
Yoshida, M., Yamashita, T., Okada, H., Oishi, N., Nio, K., Hayashi, T., Nomura, Y., Hayashi, T., Asahina, Y., Ohwada, M., 2017. Sorafenib suppresses extrahepatic metastasis de novo in hepatocellular carcinoma through inhibition of mesenchymal cancer stem cells characterized by the expression of CD90. Sci. Rep. 7, 11292.
Jiang, C., Xu, R., Li, X.-X., Zhou, Y.-F., Xu, X.-Y., Yang, Y., Wang, H.-Y., Zheng, X.S., 2018. Sorafenib and carfilzomib synergistically inhibit the proliferation, survival, and metastasis of hepatocellular carcinoma. Mol. Cancer Ther. 17, 2610–2621.
Adilakshmi, T., Ness-Myers, J., Madrid-Aliste, C., Fiser, A., Tapinos, N., 2011. A nuclear variant of ErbB3 receptor tyrosine kinase regulates ezrin distribution and Schwann cell myelination. J. Neurosci. 31, 5106–5119.
Mahmoud, G., Jedelská, J., Omar, S.M., Strehlow, B., Schneider, M., Bakowsky, U., 2018. Stabilized tetraether lipids based particles guided prophyrins photodynamic therapy. Drug Deliv. 25, 1526–1536.